

The phase-space structure of cold dark-matter halos: Insights into the Galactic halo

Amina Helmi^{*}, Simon D.M. White[†] and Volker Springel[‡]

Max-Planck-Institut für Astrophysik, Karl-Schwarzschild-Str. 1, 85740 Garching bei München, Germany

Accepted ... Received ...; in original form ...

ABSTRACT

We study the formation of the Milky Way’s halo in a Λ CDM cosmology by scaling down a high resolution simulation of the formation of a cluster of galaxies. We determine how much phase-space substructure is left over from the objects that merge to build up the present galaxy. We study the debris streams originating from such objects and find that their evolution can be explained simply in terms of the conservation of phase-space density. Analysing the mass growth history of our halo we find that its inner regions have been in place for more than 10 Gyr, but that the growth of the halo as a whole is more gradual, in agreement with other high resolution simulations of dark-matter halos. Recent accretion contributes to the inner 10 kpc of the halo only at the 10^{-4} level. Finally we determine the number of dark-matter streams as a function of distance from the centre of the halo. In the equivalent of the “Solar vicinity”, we find that the dark-matter is smoothly distributed in space, and that the velocity ellipsoid is formed by hundreds of thousands of streams, most of which have velocity dispersions of the order of 1 km s^{-1} or less.

Key words: dark-matter – galaxies: clusters, formation, halos – methods: numerical – Galaxy: halo, formation, dynamics

1 INTRODUCTION

Over the last twenty years, the hierarchical paradigm has emerged as the standard model to describe the formation of structure in the Universe. As embodied in the current “concordance” Λ CDM model it appears to be consistent with a very wide range of cosmological data ranging from fluctuations in the Cosmic Microwave Background through the structure of Ly α forest absorption in QSO spectra and the gravitational shear induced by dark-matter structures to the observed large scale structure in the galaxy distribution. An important characteristic of such models is that they are based on a set of well-defined and testable assumptions. This renders possible the detailed modelling of the formation and evolution of galactic systems, and a later comparison to observations of the properties of these systems as a function of environment or redshift (e.g. Diaferio et al. 2001; Benson et al. 2001; Somerville, Primack & Faber 2001).

It is also possible to test the hierarchical paradigm on our Galaxy (e.g. Hernández, Avila-Reese & Firmani

2001). Several groups (Moore et al. 1999; Klypin et al. 1999; Klypin, Zhao & Somerville 2002) have focused on the properties of dark halos, hoping to constrain the nature of dark-matter. These groups performed high resolution simulations of a galactic size halo in CDM cosmologies. They confirmed earlier analytic claims (Kauffmann, White & Guiderdoni 1993) that the predicted number of satellites exceeds the known population in the Local Group by a factor of ten. Some attempts have been made to account for the disagreement, by changing the nature of the dark-matter (Spergel & Steinhardt 2000; Bode, Ostriker & Turok 2001), by modifying the initial power spectrum of density fluctuations (Kamionkowski & Liddle 2000) or by taking into account the effects of a reionising background which may inhibit star formation in the smallest mass halos (Kauffmann et al. 1993; Bullock, Kravtsov & Weinberg 2001; Benson et al. 2002). The recent results by Kleyna et al. (2002) on the mass distribution in the Draco dSph (see also Mateo 1997 and Lokas 2001 for a similar study on Fornax) favour an astrophysical explanation since the actual circular velocities of the other satellite galaxies of the Milky Way are in fact several tens of km s^{-1} larger than previously thought, and agree with those expected for the most massive substructures in a Λ CDM universe (Stoehr et al. 2002).

Broadly speaking, the hierarchical paradigm predicts that the Milky Way formed through mergers of smaller sys-

^{*} Present address: Sterrenkundig Instituut, Universiteit Utrecht, P.O.Box 80000, 3508 TA Utrecht, The Netherlands. E-mail: a.helmi@phys.uu.nl

[†] E-mail: swhite@mpa-garching.mpg.de

[‡] E-mail: volker@mpa-garching.mpg.de

tems (White & Rees 1978). These systems would contribute to the dark halo, the spheroid (the bulge and the stellar halo) and to the Galactic gas reservoir. It may be very difficult to determine the relative gas contribution of these progenitor objects to the present Galaxy, since gas “easily forgets” its site of origin. However for collisionless stars and dark-matter the situation can be quite different. If the dynamical mixing timescales are sufficiently long (i.e. longer than the age of the Universe) it may be possible to “break-up” the Galactic spheroid (stars and may be even dark matter particles) into coherent structures in phase-space directly related to the systems that merged to form the Milky Way we observe today.

A first attempt at determining whether the merging history of the Milky Way may be imprinted in the phase-space structure of *nearby* halo stars, and thus be recovered, was made by Helmi & White (1999; hereafter HW). They studied the infall of satellites onto a fixed Galactic potential, and the evolution of the debris in phase-space. They found that after 10 Gyr stars having a common origin are distributed smoothly in space, but appear very clumped in velocity space, where they define streams with very small velocity dispersions. The expected number of such streams scales with the initial size r , velocity dispersion σ and orbital period P , of the disrupted object:

$$N_{\text{stream}} \sim 10 \left(\frac{r}{1 \text{ kpc}} \right)^2 \left(\frac{\sigma}{15 \text{ km s}^{-1}} \right) \left(\frac{P}{0.23 \text{ Gyr}} \right)^{-3}. \quad (1)$$

The total number of stars associated with the object is $N_* \propto r\sigma^2$ (from the virial theorem) while the volume V over which they are spread scales with the cube of the size of the orbit, and so approximately as P^3 . Hence the number of stars per stream in the Solar neighbourhood scales as $N_*/VN_{\text{stream}} \sim \sigma/r$; objects with large initial velocity dispersion and small initial size should produce the most easily detectable streams with little dependence on initial period. Such arguments suggest that the Solar neighbourhood velocity ellipsoid is composed of 300 – 500 kinematically coherent structures which originated in past merger and accretion events. A pair of halo streams that can perhaps be directly linked to a disrupted satellite were detected in the Solar neighbourhood by Helmi et al. (1999). The progenitor of these two streams was probably similar to the dwarf galaxy Fornax. Substructure in the outer halo also appears to be ubiquitous, and has been found by several surveys over the last few years (e.g. Ivezić et al. (2000) and Yanny et al. (2000) for the SDSS; Dohm-Palmer et al. (2001) for the SPS; Vivas et al. (2001) for QUEST). Most of these recently discovered structures can be associated to just one of Milky Way’s satellites: the Sagittarius dwarf galaxy which is in the process of being completely disrupted (Ibata et al. 2001; Martínez-Delgado et al. 2001; Helmi & White 2001).

A weak point of the HW analysis and of similar studies (e.g. Johnston, Hernquist & Bolte 1996; Johnston 1998), is the assumption of a fixed, smooth potential onto which galaxies are accreted. In hierarchical clustering, galaxy potentials are constantly changing, and can vary very violently during mergers. Large numbers of clumps orbit the centre of even a “virialised” halo. These clumps may have substantial effects on the structure of debris streams (e.g Johnston, Spergel & Haydn 2002; Ibata et al. 2002; Mayer et al. 2002).

The main goal of the present paper is to understand the

phase-space structure of cold dark-matter halos. In particular, we want to study the evolution of satellite debris, and to quantify the expected amount of substructure. We also want to determine to what extent previous results are valid in the truly hierarchical regime of the build-up of a galaxy. We tackle these problems by scaling down to galactic size a high-resolution simulation of the formation of a cluster in a Λ CDM cosmology (Springel et al. 2001).

The paper is organised as follows. In Sec.2 we describe the simulations, in Sec.3 we follow the evolution in phase-space of debris streams, and compare to the analytic model of HW in Section 3.2. Sec.4 describes the mass-growth history of the simulated dark-matter halo, and in Section 5 we determine the number of streams and their internal properties as function of distance from the dark-matter halo centre. We leave the summary and discussion of our results for Section 6.

2 METHODOLOGY

2.1 The simulations

The simulation we analyse here was carried out using a parallel tree-code (Springel, Yoshida & White 2001) on the Cray T3E at the Garching Computing Centre of the Max Planck Society. Its initial conditions were generated by zooming in and re-creating with higher resolution a particular galaxy cluster and its surroundings formed within a cosmological simulation (as in Tormen, Bouchet & White 1997). The original parent Λ CDM cosmological simulation (from Kauffmann et al. 1999) had parameters $\Omega_0 = 0.3$, $\Omega_\Lambda = 0.7$, $h = 0.7$ and $\sigma_8 = 0.9$. The cluster selected for re-simulation was the second most massive cluster in this simulation, having a virial mass of $8.4 \times 10^{14} h^{-1} M_\odot$. The particles that end up in the final cluster of the cosmological simulation and in its immediate surroundings (defined by a comoving sphere of $70h^{-1}$ Mpc radius) were traced back to their Lagrangian region in the initial conditions for re-simulation. The initial mass distribution between 21 and $70h^{-1}$ Mpc was represented by 3×10^6 particles. In the inner region, where the original simulation had 2.2×10^5 particles, new initial conditions were created using 6.6×10^7 particles. Small scale power was added in accordance with the better k-space sampling allowed by the larger number of particles. The original force softening was also decreased to obtain better spatial resolution. The new simulation was run from high redshift until $z = 0$, and was analysed in considerable detail in Springel et al. (2001). In this high resolution simulation there are about 20 million particles within the virialised region of the cluster halo.

2.2 Scaling to a Milky Way halo

In Figure 1 we show the circular velocity profile of the cluster at $z = 0$. We determine the cluster centre by successively refining a mesh located on the cluster, and determining the cell containing the largest number of particles. This process is repeated until the largest number of particles in a given (now small size) cell is sufficiently small to determine by simple counts which particle has the largest number of neighbours. Its position corresponds to the point of maximum density

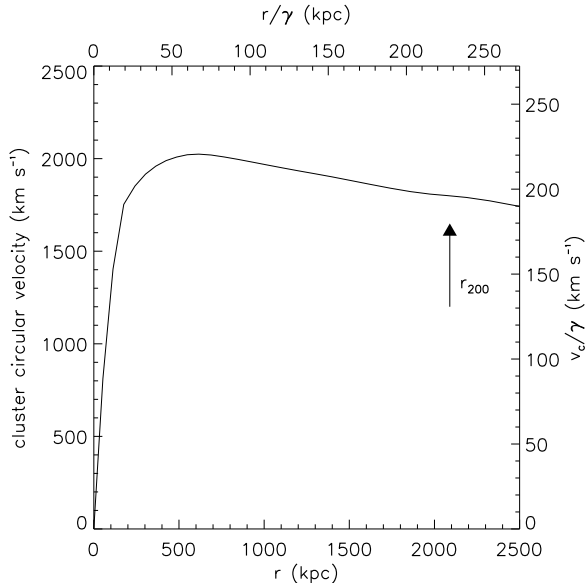


Figure 1. The circular velocity $V_c(r) = \sqrt{GM(r)/r}$ of the cluster for our simulation S4. Axes show radii and circular velocities both before and after scaling down to Milky Way size.

and it is defined as the cluster centre. This determination is robust against changes in the mesh shape and size, and we estimate the error in the final position of the centre of the cluster to be of the order of 0.7 kpc, comparable to the scale of the gravitational softening used in the simulation. The circular velocity is then determined after spherically averaging the mass distribution around the centre of the cluster and is derived from $V_c(r) = \sqrt{GM(r)/r}$. By fitting a Navarro, Frenk & White (NFW; 1996) profile, we find that the concentration of the cluster halo is $c_{\text{NFW}} = 7.3$, the scale radius $r_s = 285$ kpc and the virial radius $r_{200} = 2090$ kpc.

We can scale the cluster to a “Milky Way” halo, by requiring that its maximum circular velocity be equal to 220 km s^{-1} . The required scaling factor γ is given by

$$\gamma = \frac{V_c^{\text{cl}}}{V_c^{\text{MW}}} = \frac{r_{200}^{\text{cl}}}{r_{200}^{\text{MW}}} \sim 9.18. \quad (2)$$

With this scaling, the virial radius of our simulated Milky Way dark-matter halo is 228 kpc. Its virial mass is $1.28 \times 10^{12} M_\odot$, the mass of an individual particle is $8.66 \times 10^4 M_\odot$, and the gravitational force in the final object has an equivalent Plummer softening of 0.11 kpc.

Our argument that with the simple scaling of Eq.(2) this simulation is a fair representation of the growth of the Milky Way relies on both theoretical and numerical results (Lacey & Cole 1993; Moore et al. 1999). Numerical simulations by Moore et al. (1999) have shown that galaxy and cluster halos have similar properties in terms of final structure (density profile), number of satellites, etc., despite typically assembling at systematically different redshifts. Jing & Suto (2000) have also performed high resolution simulations of several galaxy, group and cluster size halos. Although they find that galaxy halos have a steeper inner profile than larger mass halos, they also find that the scatter in the properties of objects belonging to the same class is as large as the systematic differences between classes. We expect therefore,

that our scaled simulation will represent reasonably well the formation process of a galactic halo, except that its assembly occurs at later times than the majority of such halos. From now on we will use this scaling in the paper, and assume, unless otherwise stated, that the simulation represents a galaxy halo.

3 THE PHASE-SPACE EVOLUTION OF DEBRIS

Here we study the phase-space evolution of debris from the disrupted halos that end up forming the “Galactic” dark halo at the present time. With this goal in mind, we proceed by identifying halos at high-redshift which are directly accreted onto the main progenitor of the “Milky Way’s” halo.

We identify halos at each output time using a Friends-of-Friends (FOF) algorithm, which links particles separated by less than 20% of the mean interparticle separation. In this way we can construct a detailed merger history of the galaxy. As we step back in redshift we identify at each output the most massive halo which is part of the galaxy’s main progenitor at the subsequent time. We say that a halo identified at redshift z will be directly accreted onto the main progenitor at z' (the redshift of the next simulation output) if at least half of its particles *and* the most-bound particle have become part of the main progenitor at z' . Here the most-bound particle refers to the particle with the minimum potential energy in the (to be) accreted halo.

The centre of mass position \mathbf{p}_{CM} and velocity \mathbf{v}_{CM} of the main progenitor are computed as follows. We first determine the location of the most bound particle \mathbf{p}_{mb} . We define concentric spheres of successively smaller radii (down to 10 kpc radius) around this particle, and compute the centre of mass \mathbf{p}'_{CM} from the particles within these spheres. We stop this iterative procedure when $|\mathbf{p}_{\text{mb}} - \mathbf{p}'_{CM}| < \epsilon$, where $\epsilon = 0.3$ kpc. This is then defined as the location of centre of mass of the main progenitor. The velocity of the centre of mass is then \mathbf{v}'_{CM} , measured by the velocities of the particles within the largest sphere for which the above condition is satisfied.

This is like following the (thickest) trunk of the merger tree, which would correspond to the galaxy’s main progenitor, and studying what happens to halos which join from other tree branches as time progresses. The idea is illustrated in Figure 2.

For our high resolution simulation we have identified 752 halos with at least 1000 particles (which corresponds to a minimum mass of $8.66 \times 10^7 M_\odot$), which fall onto the main progenitor between redshift $z = 2.4$ and the present day. The accreted halos have a large spread in mass as shown in the bottom panel of Figure 3. From the top panel of this Figure we note that in some cases the satellite-to-primary mass ratio is close to unity, corresponding to a major merger. Such mergers, although few in number, contribute a substantial fraction of the total mass growth.

3.1 Spatial and kinematic evolution of halo debris

We now study in detail how the debris streams from one of the above 752 halos evolve in time. We follow a halo that merges with the main progenitor at redshift 1.8, and has

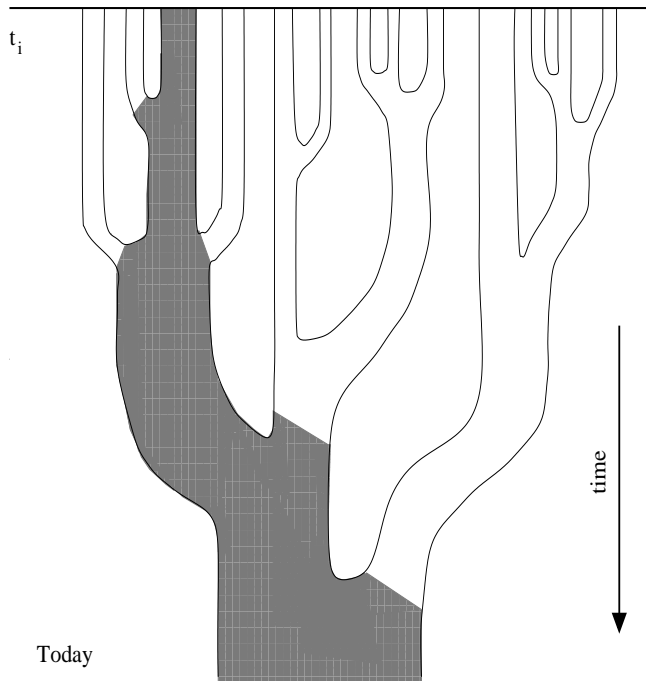


Figure 2. A schematic representation of the merger history of a galaxy. The dark trunk at any given time represents the galaxy main progenitor, and the branches linked to this trunk correspond to the halos that merge directly with the galaxy (based on Lacey & Cole, 1993).

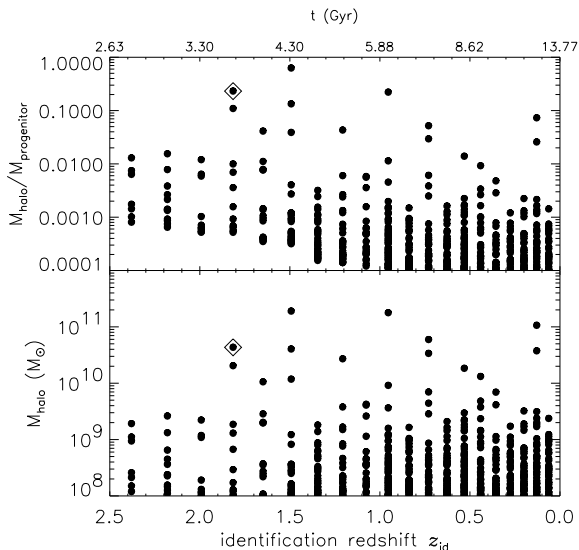


Figure 3. The top panel shows the mass ratio of the halos directly accreted onto the main progenitor as a function of their accretion time. Note that in some cases this mass ratio approaches one, meaning that the galaxy is experiencing a major merger. In the bottom panel we plot the actual masses of these halos. The diamonds are here used to denote a halo which we discuss in detail in Sections 3.1 and 3.2.

an initial mass of $4.3 \times 10^{10} M_{\odot}$. This halo is denoted with a diamond in Figure 3. Its mass at the time of accretion was about 25% that of the main progenitor. This satellite decays through dynamical friction to the centre of the main progenitor where it is fully disrupted. The mass stripped off at earlier times mainly populates the outer regions of the final object, while that lost at late times ends up closer to its centre.

3.1.1 Evolution of debris in the outer galaxy

We identify material from the accreted halo which is part of a tidal stream in the outer galaxy at the present time. We select a reference particle in this structure, which can be traced back to $z = 1.8$, and then followed forwards in time. In Figure 4 we show a time sequence of the spatial distribution of particles lost at $z = 1.8$. We say that a particle has been lost by its progenitor halo if its binding energy has become positive. The binding energy ϵ of a particle located at \mathbf{r} and with velocity \mathbf{v} with respect to the centre of mass of the satellite¹ is defined as $\epsilon = \Phi(\mathbf{r}) + 0.5|\mathbf{v}|^2$, where $\Phi(\mathbf{r})$ is the potential energy at \mathbf{r} due to all particles in the satellite. From Fig. 4 we see that the initial distribution of particles is relatively compact, and that as time passes by the material is strung out in a characteristic stream-like structure (e.g at $t = 4.31$ Gyr) over several tens to hundreds of kiloparsecs. At the final time the material appears to be more smoothly distributed over the whole box, which is 400 kpc (in physical units) on a side. Our simulations are not well-suited to address the effects of other dark-matter lumps on tidal tails (cf Johnston et al. 2001), which could be related to some of the transient structures observed in this Figure. Our main limitation is the large time interval between stored outputs which prevents us from determining the effect of close encounters and their relation to the features seen in Figure 4.

In many of the snapshots tight small substructures can be observed. These objects were already present as subhalos within the satellite halo before it was accreted by the galaxy. After accretion, they were released from their parent satellite, becoming subhalos of the main galaxy. It is worth mentioning that these subhalos only constitute a small fraction of the debris material lost by the satellite (less than 10%, e.g. Ghigna et al. 2000; Springel et al. 2001).

In Figure 5 we show the velocities of debris particles that are relatively close (inside a cube of side 20 kpc) to the reference particle, at three different times. For comparison, note that the virial radius of the satellite at the time of infall was approximately 37 kpc. The solid grey circles correspond to particles which

(i) were always neighbours of the reference particle: to be in this set, particles need to have x , y and z coordinates within 10 kpc of those of the reference particle in all previous outputs;

(ii) are within 5 kpc of the reference particle in each coordinate in the current output.

We note that the initial velocity distribution of the halo

¹ The centre of mass is here defined by the 0.1% most bound particles of the system, which in this case corresponds to 500 particles.

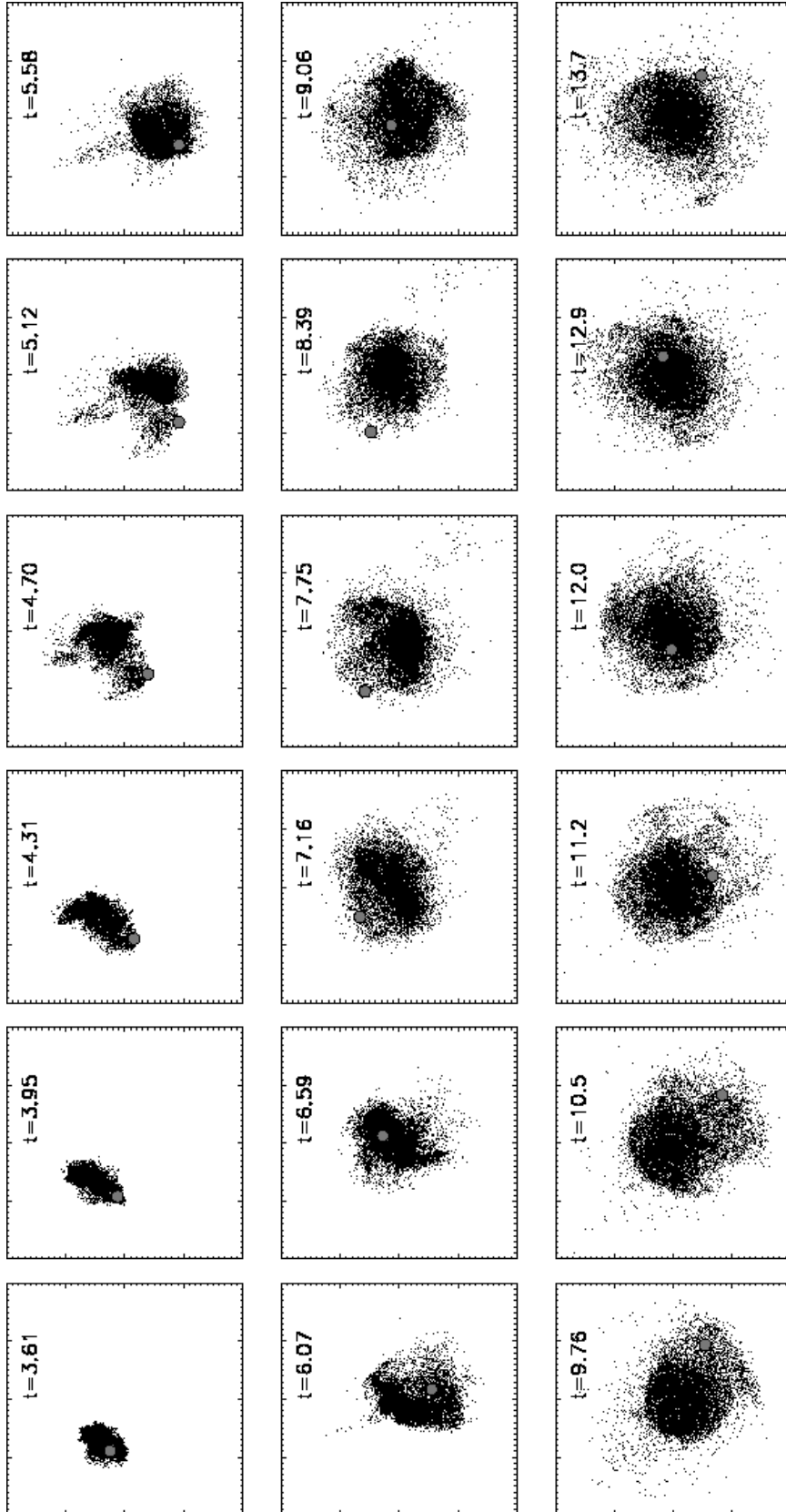


Figure 4. Evolution of the spatial distribution of particles from a halo of $4.3 \times 10^{10} M_{\odot}$ that merged at $z = 1.8$ ($t = 3.61$). We plot here the x vs z positions of the 10% of the particles that were lost from this halo at this redshift. The box is 400 kpc (in physical units) on a side, and at each output it is centred on the main progenitor's centre of mass. The grey solid circle denotes the location of the reference particle which belongs to a stream orbiting the outer galaxy.

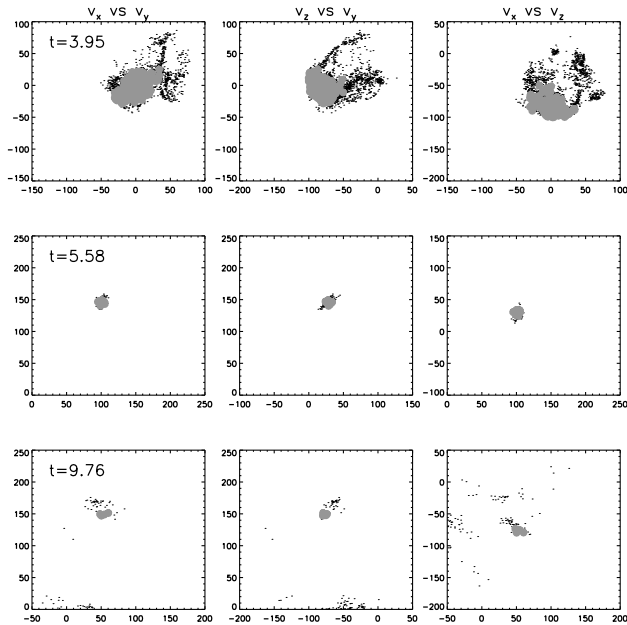


Figure 5. Evolution of the velocity distribution of neighbours of the reference particle (shown as a solid grey circle in Figure 4) of the satellite halo of the previous figure. Dots correspond to particles that fall inside a cube of side 20 kpc around the reference particle at the given time. The filled circles are particles that fall within a box of side 10 kpc, and were neighbours of the reference particle in all previous outputs. These particles define the stream in which the reference particle is located. Notice the decrease in the density and velocity dispersion of the filled circles.

is broad, and relatively clumpy. As discussed before, this clumpiness reflects the internal structure of the object that fell in. As time goes by, the motions of the neighbours of the reference particle become more similar, and the velocity-box is empty except for velocities close to that of the reference particle (middle row). At later times (bottom row), other moving groups are visible, showing that the system has now produced multiple intersecting streams even in the outer galaxy.

The evolution of the velocity dispersion σ in the neighbourhood of the reference particle is shown in the top panel of Figure 6. Here σ is defined as $\sqrt{\sigma_x^2 + \sigma_y^2 + \sigma_z^2}/\sqrt{3}$, and is therefore independent of the choice of the coordinate system. It is measured for the set of particles shown as grey solid circles in Figure 5, that is for particles that satisfy both conditions (i) and (ii) for being neighbours of the reference particle. We also measure σ for a subset of even closer neighbouring particles (whose x , y , and z coordinates in all outputs before the one under study were within 5 kpc of those of the reference particle, and in the current output are within 2.5 kpc). The different values of the velocity dispersion in the stream obtained for these two cases are due to velocity gradients, which can be as large as the measured dispersions themselves. Note as well the decrease by roughly a factor 10 in the velocity dispersions in only 2 Gyr.

The stream’s density is shown in the bottom panel of the same figure. It is measured at each output by the number of neighbours in the stream in boxes of a given size (either of 5 or 10 kpc on a side) around the reference particle. For

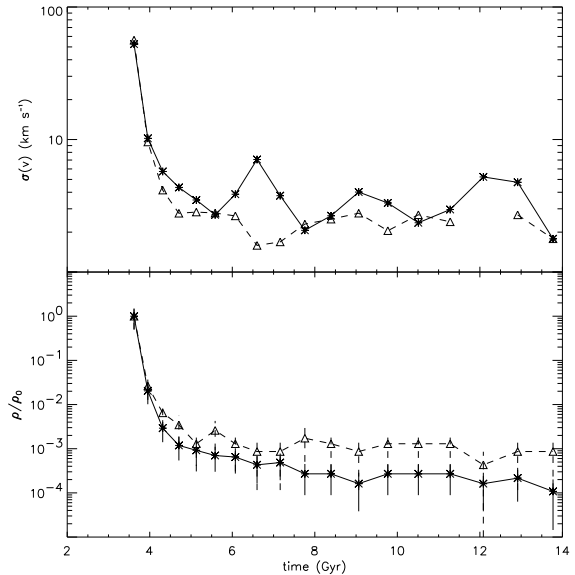


Figure 6. The top panel shows the evolution of the velocity dispersion in the neighbourhood of the reference particle of the same satellite halo as in Figures 4 and 5. The solid line corresponds to the 1-d velocity dispersion computed from the particles shown as grey solid circles in Fig. 5. The dashed curve is for a subset which are even closer to the reference particle, within a box of side 5 kpc. The differences can be attributed to gradients along the orbit, which are particularly important at late times. The bottom panel shows the evolution of the density of the stream defined by the same set of particles used in the top panel. The long term behaviour is probably not physical, especially in the case of the smaller box, but is dominated by Poisson noise in the number of particles counted.

the larger volume, this number evolves from being slightly larger than five thousand to only thirteen after less than 2 Gyr of evolution. This implies that after this time, the number counts are dominated by Poisson noise.

3.1.2 Evolution of debris closer to the centre of the galaxy

To follow the evolution of streams closer to the centre of the galaxy we focus on material lost a few Gyr after the satellite halo shown as a diamond in Fig.3 was accreted. We here focus on debris lost from this satellite halo at $t = 7.16$ Gyr, or 3.5 Gyr after infall. This is deposited at an intermediate distance from the centre of the galaxy. We decided against tracking material lost even later because it turns out to be very difficult to follow streams from such material with our numerical resolution and number of stored outputs. The material lost at later times mixes on shorter timescales. Streams more rapidly reach very small densities, and we are unable to determine their properties reliably.

Figure 7 shows the evolution of the spatial distribution of the particles lost at $t = 7.16$ Gyr. Note that the particles are more smoothly distributed than in the case of the outer halo material shown in Figure 4. This is because the inner regions of (satellite) halos are in general much less lumpy than the outskirts due to the shorter dynamical timescales.

As in the previous section we choose a reference particle (amongst all those lost at $t = 7.16$ Gyr) that orbits through

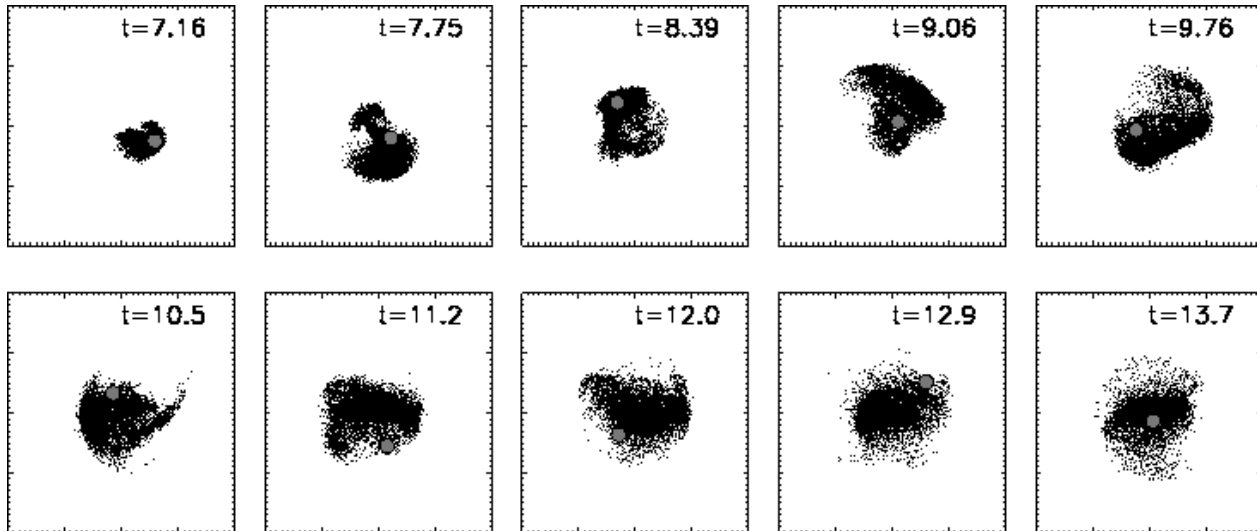


Figure 7. Evolution of the spatial distribution of particles from a halo of $4.3 \times 10^{10} M_{\odot}$ that merged with the galaxy at $z = 1.8$. We plot here only 25% of the particles lost from this halo 3.5 Gyr after infall (6.6 Gyr ago). As in Figure 4, the box is 400 kpc on a side in physical units, and its origin coincides with the position of the main progenitor’s centre of mass at all times. We only show the x (horizontal axis) vs y (vertical axis) projection. The material lost at this time is deposited within about 100 kpc from the galaxy’s centre, much closer than that lost at earlier times (for comparison see Fig.4). We note that there is a fairly sharp cutoff in the density at that radius. This corresponds roughly to the apocentre of the orbit of the satellite at the time these particles were released. The grey solid circle shows the location of the reference particle which belongs to a stream orbiting the “intermediate” galaxy at the present time.

the intermediate regions of the galaxy. Proceeding as before, we follow the evolution of the velocities of particles located close to the reference particle at all times. Figure 8 shows the velocity distribution in the neighbourhood of the reference particle. By comparing to the analogue for the outer halo stream (Fig. 5) we note that, not just the spatial distribution, but also the velocity distribution is much smoother initially. This is also true at late times, and very rapidly a regime is reached where multiple streams can be observed. Figure 9 corresponds to the evolution of the velocity dispersion and density of a stream. Again we are not able to follow the evolution of the velocity dispersion of the stream at late times, because we run out of neighbouring particles quite rapidly, particularly for the smaller box. After $t = 10.5$ Gyr, or 2 Gyr of evolution, the number of neighbours is dominated by Poisson noise. After this time, the values of the 1-d velocity dispersion, when measured, are based on the velocities of only two or three particles.

The evolution of the intermediate and outer halo streams is characteristic of all streams originating in directly accreted halos. Naturally the properties of streams and their location in the galaxy halo will depend on their progenitor, in particular on its initial mass. In this respect, streams originating in smaller halos are narrower, more clearly defined, and, typically, they phase-mix on longer timescales.

3.2 Mixing in phase-space: Comparison to analytic models of stream evolution

In the previous section we found a very rapid decline in the density and velocity dispersion of streams, especially in the first few Gyr of evolution. After this initial period, the number of particles in a stream is so small in our simulation that it is dominated by Poisson noise. In this regime, it is difficult to quantify the properties of the stream, and it is

therefore hard to determine whether the lack of variation of the velocity dispersion at late times is due to numerical limitations or is a real effect.

To gain insight into these issues, we will analyse the expected behaviour of streams evolving in a smooth time-independent potential, which should resemble that of the galaxy halo. Using the approach developed by HW, we can follow the evolution of streams produced in a spherical and static NFW potential. The basic idea here is to map the initial system onto action-angle space, then follow the much simpler evolution in this space, and finally transform back *locally* onto observable coordinates (all these being linear transformations; for details see HW). This method, which uses action-angle variables, is limited to applications in which the potential is separable (cf Goldstein 1953; Binney & Tremaine 1987). This includes all spherically symmetric potentials but only few axisymmetric and triaxial ones, such as the general class of Stäckel potentials (e.g. Lynden-Bell 1962; de Zeeuw 1985; Dejonghe & de Zeeuw 1988).

We also approximate the phase-space density around the reference particle by a multivariate Gaussian distribution. This is possible because the multivariate Gaussian is determined from the properties of particles in a volume much smaller than the size of the halo.

As discussed in Section 2.2, the (galaxy) halo can be fit by an NFW profile:

$$\rho(r) = \rho_0 \frac{\delta_c r_s^3}{r(r+r_s)^2}, \quad (3)$$

where $\rho_0 = 3H^2(z)/(8\pi G)$ and δ_c is a function of the concentration of the halo $c_{\text{NFW}} = r_{200}/r_s$:

$$\delta_c = \frac{200}{3} \frac{c_{\text{NFW}}^3}{\log(1+c_{\text{NFW}}) - c_{\text{NFW}}/(1+c_{\text{NFW}})}. \quad (4)$$

Recall that $H(z) = H_0 \sqrt{\Omega_{\Lambda} + \Omega_0(1+z)^3}$. The potential as-

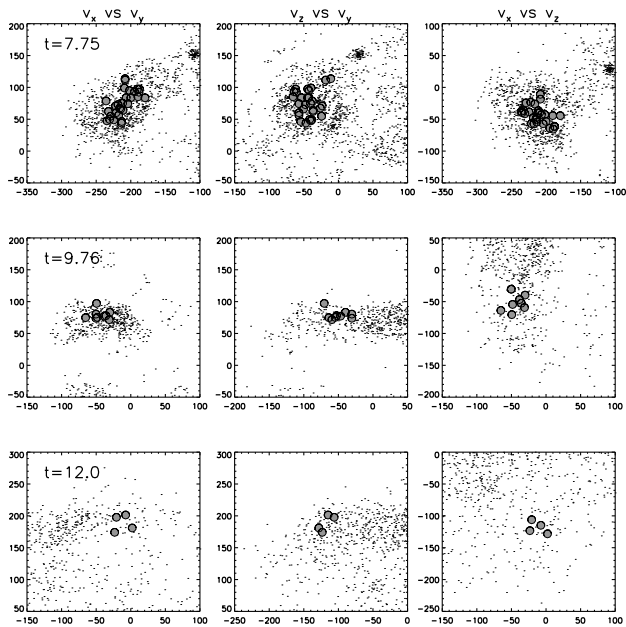


Figure 8. Evolution of the velocity distribution of neighbours to the reference particle of the same halo as before, where the reference particle orbits the intermediate regions of the galaxy at the present time. Dots correspond to particles that fall within a box of side 20 kpc from the reference particle in the output shown. The solid grey circles correspond to particles that fall within a box of side 10 kpc, and were also neighbours of the reference particle at all previous times. They define the stream to which the reference particle belongs.

sociated with this density can be obtained by integrating Poisson’s equation, and is found to be:

$$\Phi(r) = -\Phi_0(z) \frac{r_s}{r} \log \left(1 + \frac{r}{r_s} \right). \quad (5)$$

Here $\Phi_0(z) = 3/2 H^2(z) \delta_c r_s$. The values of the parameters r_s and r_{200} given in Section 2.2 should be multiplied by the factor γ for the scaled halo.

In this (spherically averaged) potential we integrate the orbit of the reference particle in time. This integration is done in two complementary ways:

(i) starting from the position and velocity of the reference particle at the “time of formation of the stream” (this is the time when the particles become unbound from their parent halo). In this case, the integration is performed forwards in time, and the potential used is given by Eq. (5), where z is the redshift of formation of the stream.

(ii) starting from the position and velocity of the reference particle at the present time. The orbit is then integrated backwards in time, until the “time of formation of the stream”, in the present-day potential ($z = 0$).

In both cases, the orbits are integrated in the reference frame of the centre of mass of the main progenitor of the galaxy.

In the top panel of Figure 10 we plot the radial oscillations of the orbit for the outer halo reference particle. The solid curve corresponds to the NFW potential at redshift $z_{\text{form}} = 1.8$, while the dashed curve to that at $z = 0$. We note that for the reference particle in the outer halo stream, the best agreement is obtained when the integration is per-

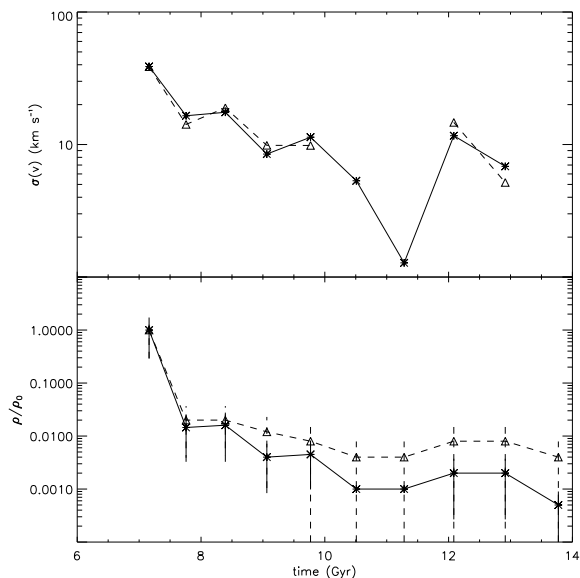


Figure 9. The top panel shows the evolution of the 1-d velocity dispersion in the neighbourhood of the reference particle of the same halo as in the previous figure, and for a stream orbiting the “intermediate” regions of the galaxy at the present time. The solid curve corresponds to the particles shown as grey solid dots in Fig. 8, whereas the dashed curve corresponds to a subset of these located in a volume of side 5 kpc around the reference particle. The difference between the dashed and solid curves is due to velocity gradients which are dominant in these relatively large boxes. The bottom panel shows the evolution of the density of the stream of the top panel. The error bars are estimates of the noise based on Poissonian counts. Note that the values of the velocity dispersion after 10.5 Gyr are determined from the velocities of just two or three particles.

formed backwards in time. We also note that the potential seems to have fluctuated dramatically until $t \sim 6$ Gyr, inducing strong changes in the radial oscillations of the reference particle. As a whole, the orbit has evolved to a more bound state, due to the aggregation of mass during mergers.

The analogous plots for the reference particle orbiting the intermediate halo are shown in the bottom panel. Recall that here $z_{\text{form}} = 0.73$. In this case, none of the proposed orbits fit the actual orbit very well; it may be considered to lie in between these two cases. Thus, the characteristics and the evolution of the debris streams predicted for the two proposed orbits may perhaps encompass the actual behaviour of the streams in our simulations. In this “intermediate halo” case, we do not find a clear indication of evolution in the orbit. This is likely due to the mild increase in the mass within the orbit since z_{form} (see Sec. 4)

In Figures 11 and 12 we show the predicted evolution of the 1-d velocity dispersion and the behaviour of the density in the spherical static NFW potential for the outer and intermediate halo streams, respectively. The actual behaviour of the streams in the simulation is also shown for direct comparison. In both cases, we find that the decrease observed in the simulated streams is close to what is predicted for the evolution of streams moving in a static potential. This is the case at least for the first few Gyrs of evolution. Although after this period we expect some differences, due to

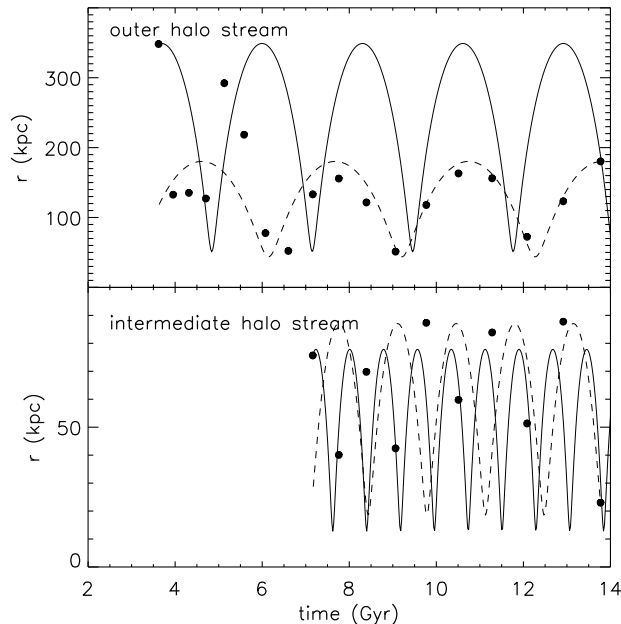


Figure 10. The top panel shows the distance r from the centre of mass of the galaxy as a function of time t for the reference particle in the outer halo stream (solid circles). The dashed line corresponds to $r(t)$ for an orbit integrated in the present-day NFW potential of the galaxy, starting from the present-day position of this particle. The solid line corresponds to an orbit in an NFW potential determined at the redshift of formation of the stream (according to Eq.5). The bottom panel shows the corresponding $r(t)$ from the simulation and the proposed orbits for the reference particle moving in the intermediate regions of the galaxy halo at the present time.

the fact that the orbit evolves in shape, the agreement still appears to be quite good. We predict a rapidly varying velocity dispersion (and density) on top of a secular evolution. The spikes take place when particles in a stream go through a caustic surface defined by their orbital turning points. To observe this behaviour in the simulation would require output times spaced by $1/2$ of the radial period at most, or roughly 0.25 Gyr for the stream orbiting the intermediate regions of the halo. Our outputs, on the other hand, are logarithmically spaced in the cosmological expansion factor $a(t)$, so that at $z = 1$ the time elapsed between two outputs is $\Delta t = 0.52$ Gyr, and by $z = 0$, $\Delta t = 0.86$ Gyr.

4 MASS GROWTH HISTORY OF THE GALAXY

Here we focus on determining the mass growth history of the halo as a function of distance from the halo centre. This is relevant in two different ways. First, debris from satellites accreted at late times will be generally less mixed, and could thus produce more massive streams. Determining where to expect these streams will enable us to understand the properties of the dark halo of our Galaxy. Secondly such satellites will have had more time to form stars in them (prior to their merging), thereby providing the galaxy with younger stars. The time of merging could thus be used as an indicator of

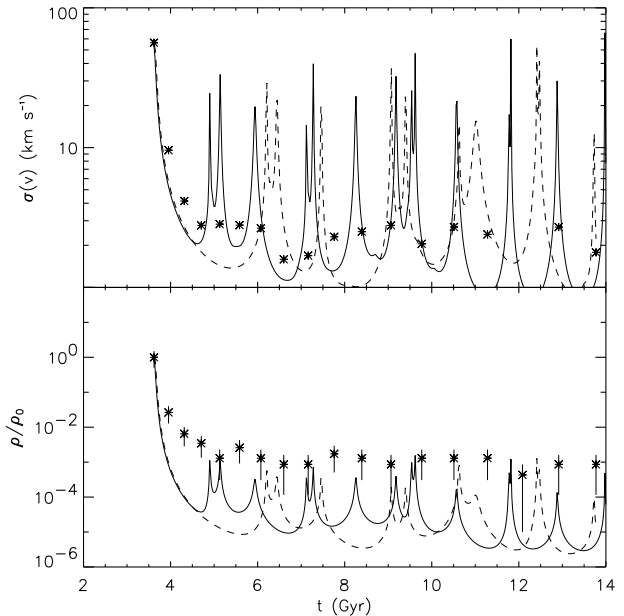


Figure 11. The phase-space behaviour predicted for the outer halo debris stream in a static NFW potential. The top panel shows the time evolution of the 1-d velocity dispersion, and the bottom panel the behaviour of the density for this stream. In both plots, the dashed curve has been computed for the present-day NFW potential, while the solid curve corresponds to the evolution in the NFW potential of the time of formation of the stream. The observed properties of the stream in the simulation are shown as asterisks and were determined from all particles within a box of side 5 kpc centred on the reference particle.

the expected age distribution of stars in different regions of our Galaxy.

We select all satellites that merged with the galaxy since redshift $z = 2.4$, and determine when these mergers took place and what is their final debris distribution. We proceed by dividing the halo in six spherical shells around the galaxy centre. These shells are located at: $r < 10$ kpc, $10 \leq r < 25$ kpc, $25 \leq r < 50$ kpc, $50 \leq r < 75$ kpc, $75 \leq r < 100$ kpc and $100 \leq r < 200$ kpc. For each particle in a given shell, we determine when it was accreted by the main progenitor of the galaxy. In Figure 13 we show the fraction of mass accreted normalised to the present mass for each shell as a function of redshift (and time). We note that the formation time of the inner galaxy is strongly biased towards high redshifts, with more than 60% of the mass already present at $z = 2.4$ or 11 Gyr ago. Conversely, we find that mergers in the last 3 Gyr, contributed a relatively small amount of mass, less than 0.1%, to this region of the galaxy halo. For the outer regions of the galaxy, we note that the growth is much more gradual in time, with accretion being almost equally important at all times.

Of course, the detailed shape of the mass growth history depends on the detailed merger history of the halo, since the peaks observed in the different histograms correspond to individual mergers taking place at those times. Nonetheless, several authors have found that there is an almost “universal” form of the mass accretion histories of galaxies and galaxy clusters (e.g. van den Bosch 2002; Wech-

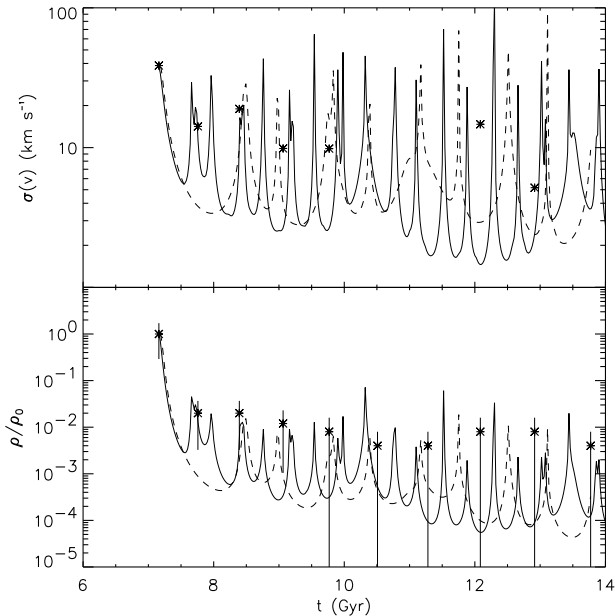


Figure 12. The phase-space behaviour predicted for the intermediate halo debris stream. The top panel shows the time evolution of the 1-d velocity dispersion, and the bottom panel the behaviour of the density for this stream. The solid curve has been computed using the NFW potential at $z = 0.73$, while the dashed curve corresponds to that at the present-day. The observed properties of the stream in the simulation are shown as asterisks and were determined from all particles within a box of side 5 kpc centred on the reference particle.

sler et al. 2002), which would also represent reasonably well the growth of our simulated halo. On the other hand, Zhao et al. (2002) have shown using high-resolution simulations that the mass in the inner regions of dark-matter halos (which they define as the mass within a scale radius, which in our case corresponds to approximately 30 kpc), is generally in place by $z \sim 2$. These results suggest that the formation history of our simulated halo is rather typical.

Another way of understanding the age structure of the galaxy halo is by focusing on what fraction of the mass was in place by different redshifts as a function of distance from the galaxy centre. To some extent this is the cumulative distribution of the plots shown in Fig. 13 for each shell. We focus on the fraction of the present-day mass in the shell that was in place at four different redshifts $z = 2.4, 1.5, 0.84,$ and 0.35 . The results are shown in Figure 14. Again we notice that 60% of the mass in the inner galaxy was in place by $z = 2.4$, and more than 90% by $z = 1.5$, i.e. 9.5 Gyr ago. Thus any accreted stellar populations in the inner regions of the galaxy are predicted to be old. On the other hand, only about half of the particles in the intermediate regions of the galaxy were present 9.5 Gyr ago (90% by $z = 0.84$). The formation of the outer galaxy is more biased towards late times, with half of its particles coming into place in the last 7 Gyr.

As a cautionary remark, let us recall that although we discuss here the expected “stellar” populations, we are actually describing the growth in mass of the dark-matter halo, rather than of the stellar halo. To describe properly the age

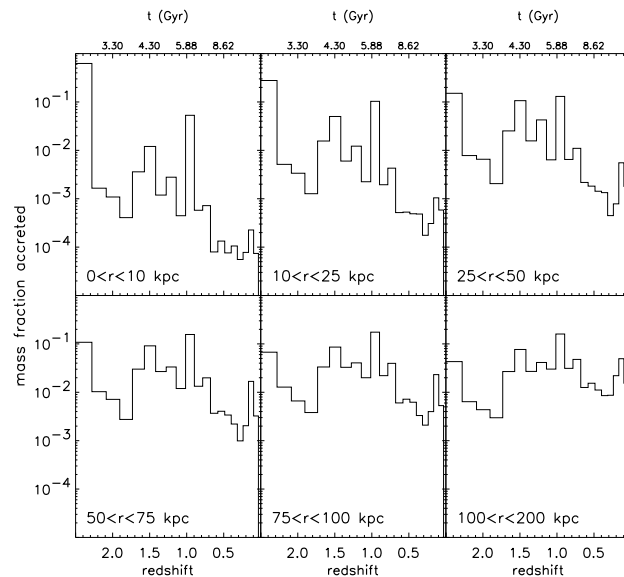


Figure 13. Growth of mass in different spherical shells around the galaxy centre. We notice here that a large fraction of the mass in the inner galaxy was already in place 10 Gyr ago. For the outer galaxy (bottom panels), the growth of mass is more gradual.

distribution of the stellar halo we would need to take into account that the stars in the different satellites that merged to build up the halo probably were located primarily in their innermost regions. This would mean, as shown in Section 3, that they should end up closer to the galactic centre than most of the dark-matter particles of the same satellite (see also White & Springel 2000). Moreover, we are also ignoring the fact that satellites orbiting the intermediate and outer regions of the halo can survive until the present day. In those cases it is possible that they continue to form stars, even while orbiting inside the dark halo of the galaxy (like the Magellanic Clouds). This means that the material that is stripped off from these systems could also contain younger stars.

5 THE NUMBER OF STREAMS

The results obtained in Section 3 suggest that the number of streams in the inner galaxy, and in particular in the vicinity of the Sun should be quite large. In this section we will estimate this quantity, as well as other characteristics of the streams, such as internal velocity dispersion and density. We will compute the number of streams inside cubes located in the inner $([-60, 60])^3$ kpc³ in the scaled “Milky Way” halo. We partition this space into boxes of 2 kpc on a side.

5.1 General definitions

Let there be L separate true streams in a given box, each having mass ν_k ($k = 1, L$). Let us assume that the observed number of particles in a stream follows a Poissonian distribution, and that the actual count is N_k particles ($k = 1, L$). Then the expectation value of N_k is $\langle N_k \rangle = \nu_k$,

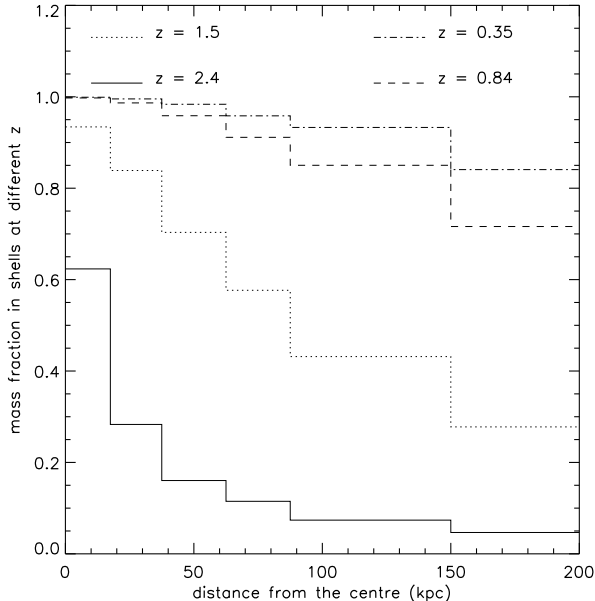


Figure 14. Mass fraction present for four different redshifts as a function of distance from the galaxy centre.

and $\langle N_k^2 \rangle = \nu_k + \nu_k^2$. (Here we measure mass in units of the particle mass of the simulation.)

The mass-weighted mean mass per stream μ is

$$\mu = \frac{\sum_{k=1,L} \nu_k^2}{\sum_{k=1,L} \nu_k}. \quad (6)$$

Therefore our estimate for μ corrected for Poisson noise will be

$$\hat{\mu} = \frac{\sum_{k=1,L} (N_k^2 - N_k)}{\sum_{k=1,L} N_k}. \quad (7)$$

In the limit of very massive streams, the Poisson correction will be negligible since $N_k^2 \gg N_k$. In the limit of small number of particles per stream, the correction will be of the same order as the quantity we measure. Note as well, that streams which in this realization do not have any particle or just have one, do not contribute to the numerator of Eq. (7). However single particle streams do contribute to the total number of particles in the box. If in a box we find mostly one-particle streams, then $\hat{\mu}$ can (correctly) become very small.

We define the mass-weighted number of streams F in a box as the ratio of the total mass in the box to the mass-weighted mean mass μ per stream in the box. Therefore F is

$$F = \frac{\sum_{k=1,L} \nu_k}{\mu}, \quad (8)$$

and our Poisson corrected estimate of F is

$$\hat{F} = \frac{\sum_{k=1,L} N_k}{\hat{\mu}},$$

or

$$\hat{F} = \frac{\left(\sum_{k=1,L} N_k \right)^2}{\sum_{k=1,L} (N_k^2 - N_k)}. \quad (9)$$

For example, if in our realization all of the streams have only two particles $N_k = 2$, our estimate of the mass-weighted filling factor becomes $\hat{F} \sim N_T$, where N_T is the total number of particles in the box. In the regime where one massive stream dominates the distribution, $\hat{F} \sim N_T / (N_T - 1)$ and will thus be close to unity. Also note that \hat{F} can be larger than N_T which will happen when most of the streams contain only 1 particle.

5.2 The minimum number of streams: the number of halos

We would like to obtain an estimate of the number of disrupted halos contributing to the density at each location in the galaxy. This is a lower limit to the total number of streams present, since a halo can (and usually does) give rise to multiple and spatially overlapping structures, as shown in Sec. 3. This lower limit will be particularly unrepresentative of the true number of streams in the inner halo both because of the very short dynamical timescales there and because more than 60% of the mass in this region comes from just one object identified at $z = 2.4$, as shown in Sec.4.

To obtain an estimate of the number of halos contributing to any given position in the Galaxy, we determine which of the halos identified at $z = 2.4$ contribute to each given box and with how many particles. In Figure 15 we plot the (Poisson corrected) mass-weighted mean number of particles per halo $\hat{\mu}_{\text{halo}}$ as a function of distance from the galaxy centre for each of the boxes considered. The thick black line corresponds to the mean number of particles in a box, averaged over all boxes at the same location. This Figure shows that most of the particles in the inner galaxy come only from a handful of disrupted halos. This can also be seen from Figure 16, where we plot the Poisson corrected estimate of the mass-weighted number of halos \hat{F}_{halo} as a function of distance from the galaxy centre and for each one of the boxes considered. We note that the mean number of halos per box in the outer galaxy is large, but that each contributes only a handful of particles. However, the inner galaxy is dominated by just a few halos making up most of the mass. This trend (of increasing number of halos with distance) is due to a form of mass segregation: heavy halos can sink by dynamical friction in short timescales to the centre of the newly formed system, whereas lighter halos, unable to decay quickly, can only deposit their mass in the outskirts.

5.3 The observed number of streams in the simulations

In general, a stream may be defined by those particles having the same orbital phase and coming from the same halo at some initial (high) redshift. The orbital phase of a particle may be determined, in principle, by counting how many times it has crossed the planes $x = 0, y = 0, z = 0$. However, because of the limited number of outputs which are logarithmically spaced in the expansion factor, it is difficult to carry this through correctly. As in section 3, we therefore define a stream as a set of particles which

- (i) have been neighbours in all previous outputs;
- (ii) are relatively close in space at the present time.

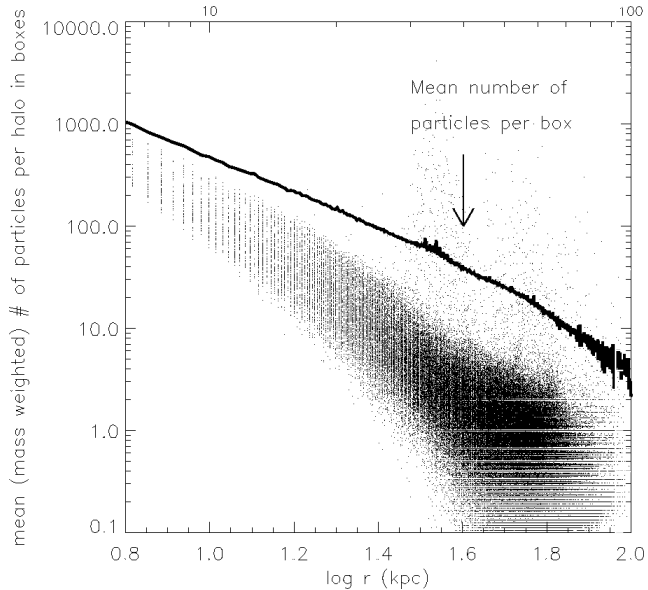


Figure 15. The mass-weighted mean number of particles from halos identified at $z = 2.4$, in boxes of side 2 kpc as a function of distance from the centre of the galaxy halo. The black curve shows the mean number of particles in these boxes averaged over all boxes at the same distance from the halo centre.

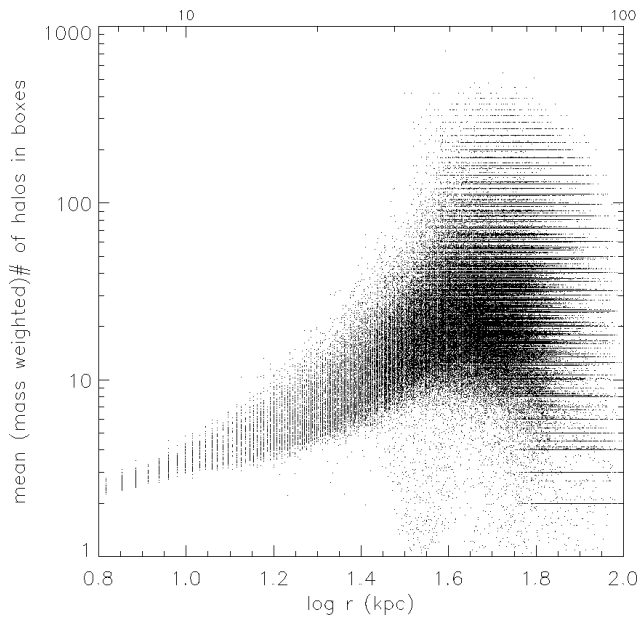


Figure 16. The mass-weighted number of halos in boxes of 2 kpc on a side as a function of distance from the centre of the galaxy halo.

In practice, we make a coarse partition of the 3-dimensional space, whose elements are boxes of 15 kpc on a side. At each output, we check in which box of the partition any given particle is located. We tag the particle by this box ID, and by the IDs of those nearest to it. So for example, a given particle will generally not be located right at the centre of a box, but will be closer to one of its edges. Thus, this particle is assigned six different numbers (corresponding to the IDs of eight neighbouring boxes) for every output, as shown in Figure 17 for the two-dimensional analogue. We

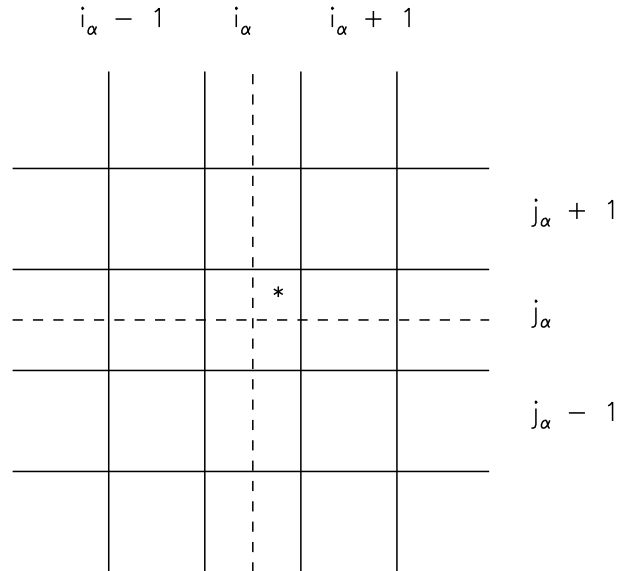


Figure 17. Here we show how we tag each particle with six different numbers, which are eventually used to determine which particles belong to the same streams. Let the asterisk indicate the position of particle α at a certain output. The box in which this particle is located has ID= $(i_\alpha, j_\alpha, k_\alpha)$. The closest boxes to the particle have $i_\alpha + 1$, and $j_\alpha + 1$, and for example $k_\alpha - 1$ in the third dimension. For another particle β to be a neighbour of the particle under analysis, it ought to have $i_\beta = i_\alpha$ or $i_\beta = i_\alpha + 1$, $j_\beta = j_\alpha$ or $j_\beta = j_\alpha + 1$, and $k_\beta = k_\alpha$ or $k_\beta = k_\alpha - 1$.

repeat this procedure for each output of our simulation. Particles which are on the same stream should have the same box tags or have been in neighbouring boxes at all previous outputs. This is almost equivalent to defining a box of 15 kpc on a side around each particle at each output, and finding which particles fall within that region. Our procedure is however, much more efficient computationally.

For the output corresponding to the present day, and for each particle in one of the 2 kpc boxes of the partition of the dark-matter halo, we find which other particles in that same box, satisfy condition (i) above (condition (ii) is automatically fulfilled). Thus at the end we obtain a link list, where particles have the same tags if they belong to the same stream.

In Figure 18 we plot the (Poisson corrected) mass-weighted mean mass per stream $\hat{\mu}$ as a function of distance from the galaxy centre for each one of the boxes considered. This Figure shows that $\hat{\mu}$ is generally smaller than unity. This happens when inside a box there are one or two streams with several particles, and the rest are one-particle structures. Clearly this is the case for the vast majority of the boxes. However, at larger distances from the Galactic centre, massive streams can be found.

In Figure 19 we plot the Poisson corrected estimate of the mass-weighted number of streams \hat{F} as a function of distance from the galaxy centre and for each one of the boxes considered. The thick grey line shows the median value of \hat{F} , where we consider all boxes located at the same distance from the centre. For the ‘‘Solar neighbourhood’’ the estimate of the mass-weighted number of streams is roughly 2×10^5 streams, showing that the local dark halo of the galaxy is extremely well-mixed. The variations in the number of streams

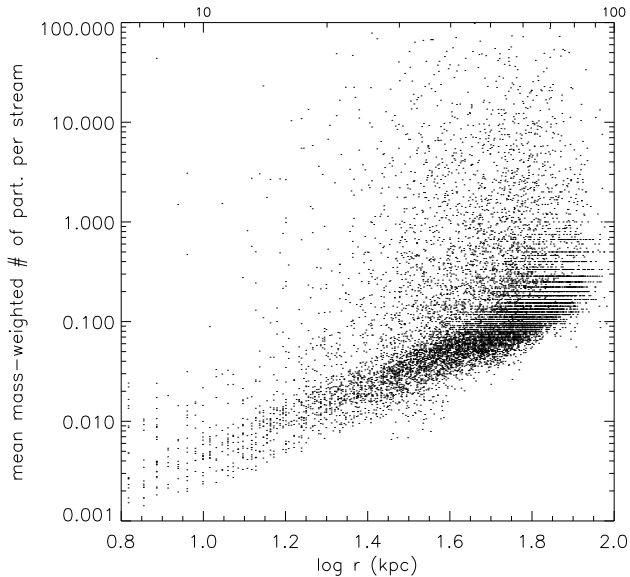


Figure 18. The mass-weighted mean number of particles for streams in boxes as a function of distance from the centre of the galaxy halo. The boxes are 2 kpc on a side.

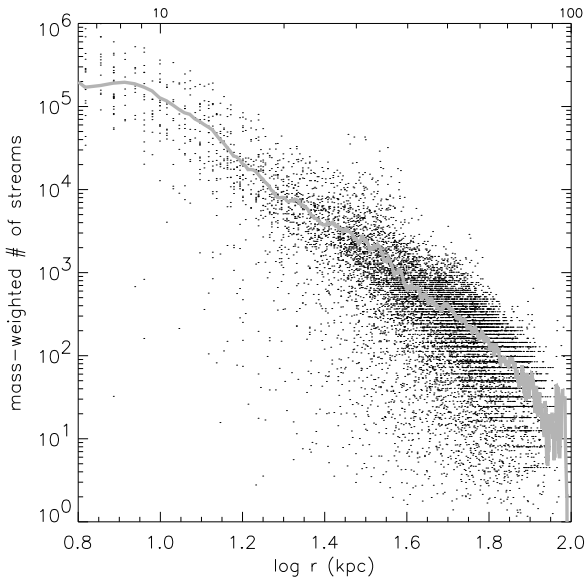


Figure 19. The mass-weighted number of streams in boxes of 2 kpc on a side for our simulation S4 as a function of distance from the centre of the galaxy halo. The dark thick line corresponds to the median mass-weighted number of streams derived for boxes at the same distance from the galaxy centre.

at fixed distance from the galaxy centre are due to variations in the number of particles themselves. These result from the flattened shape of the galaxy halo.

5.4 An analytic estimate for the number of streams

It may at first seem counterintuitive to find a number of streams larger than the number of particles actually ob-

served in a box. This effect is due to the small number of particles populating each stream, which boosts up the Poisson correction. It is fair to say that the number of streams we are determining is based on the actual presence of a few hundred streams, each detected with only two or three particles, in the inner 30 kpc region of the halo.

To ensure that the determination is meaningful we estimate how many streams we expect to find using the analytic prescription for the evolution of streams developed by HW. In Sec.3 we saw that this prescription does represent a reasonable approximation to the evolution of debris streams, even during the hierarchical build up of a CDM halo, such as that studied here.

To obtain an analytic estimate for the number of streams expected in a given box we proceed as follows:

- (i) We select 20 representative boxes at different distances from the halo centre.
- (ii) We identify the progenitor halos of the individual particles in each of these boxes.
- (iii) Among the particles belonging to the same progenitor halo, we select, when possible, 10 particles (for boxes out to $r \sim 30$ kpc). In all other cases, we choose 2 particles, or just 1, if this is all the halo contributes.
- (iv) For each of these particles we integrate the orbit:

- forwards in time: starting from the position and velocity of the particle at $z = 2.4$, using the NFW spherical potential of Eq.5 with $\Phi_0(z = 2.4)$;
- backwards in time, until $z = 2.4$, starting from the current position and velocity of the particle. In this case we use the NFW spherical potential approximation to the present-day halo.

(v) Once the orbit is known we can compute the evolution (always forwards in time) of the density in the stream where the particle is located. This is done using the action-angle formalism of HW.

(vi) From the median (in time) density of a stream² we determine the number of streams from a given progenitor halo. The number of streams is given by the ratio of the mean (coarse-grained) density of the debris to the actual density of the stream where the particle i is located, i.e.

$$N_{\text{stream},i}^{\text{halo}} = \frac{M^{\text{halo}}}{V_{\text{orb}}} \frac{1}{\rho_{\text{stream},i}(t)}. \quad (10)$$

Here $M^{\text{halo}} = 4\pi/3r_{200}^3 \langle \rho^{\text{halo}} \rangle$, $V_{\text{orb}} \sim 4\pi/3r_{\text{apo},i}^3$, and $\rho_{\text{stream},i}(t) = \rho_0 f_i(t)$, where we assume $\rho_0 \sim \langle \rho^{\text{halo}} \rangle$. Therefore we can express the number of streams as

$$N_{\text{stream},i}^{\text{halo}} = \left(\frac{r_{200}^{\text{halo}}}{r_{\text{apo},i}} \right)^3 \frac{1}{f_i(t)}. \quad (11)$$

(vii) Having obtained the number of streams for each particle, we derive the average number of streams for each halo from all n_p^{halo} particles that fall within the same box and belonged to this same halo:

² As discussed in Sec.3.2 the density of a stream oscillates strongly in time. We choose to take the median density over all its possible values in the time interval since $z = 2.4$, to avoid being dominated by a peak value just at the present time.

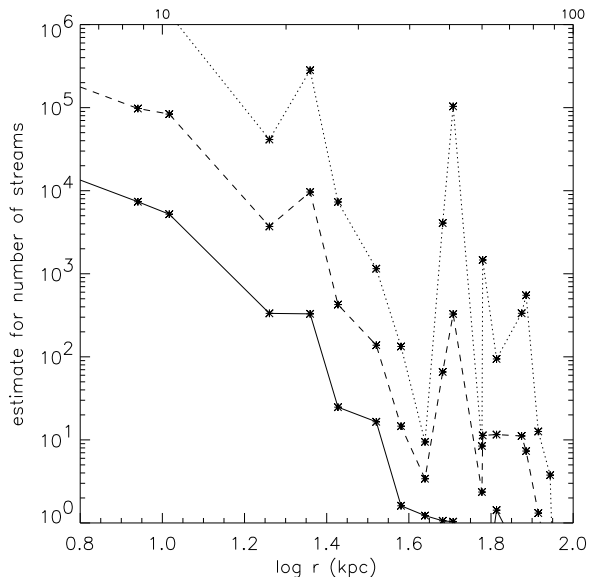


Figure 20. The estimated number of streams as a function of distance from the centre of the galaxy halo. This is derived using an action-angle formalism developed by HW, which allows one to determine the evolution of the density of a stream as a function of time in a given potential. The solid and dotted lines are computed for NFW spherical potential approximations to the properties of the halo at the present-day and at $z = 2.4$, respectively. The initial conditions of the particles’ orbits are given either by their present-day locations or by their locations at $z = 2.4$. The dashed curve is our best estimate for the number of streams, and is the geometric mean of the solid and dotted curves.

$$N_{\text{stream}}^{\text{halo}} = \frac{1}{n_{\text{p}}^{\text{halo}}} \sum_{i=1}^{n_{\text{p}}^{\text{halo}}} N_{\text{stream},i}^{\text{halo}}. \quad (12)$$

(viii) The total number-weighted number of streams in a box is now obtained by adding over all halos contributing to the box, where the weights are given by the number of particles from each halo in the box $n_{\text{p}}^{\text{halo}}$:

$$N_{\text{stream}} = \frac{\sum_{\text{halos in box}} \left(n_{\text{p}}^{\text{halo}} N_{\text{stream}}^{\text{halo}} \right)}{\sum_{\text{halos in box}} n_{\text{p}}^{\text{halo}}}. \quad (13)$$

In Figure 20 we plot our estimate for the number of streams as a function of distance from the Galactic centre. The solid curve corresponds to the estimate obtained by integrating the orbit backwards in time, from the present day conditions. The dotted curve, on the other hand, corresponds to the orbit integration performed forwards in time from $z = 2.4$. The geometric mean of these two estimates is the dashed curve in the same figure. The predicted number of streams given by the geometric mean is in reasonable agreement with what was shown in Figure 19.

5.5 Characteristics of the streams

Another interesting quantity which we can calculate for each box is the characteristic mass-weighted dispersion within a stream:

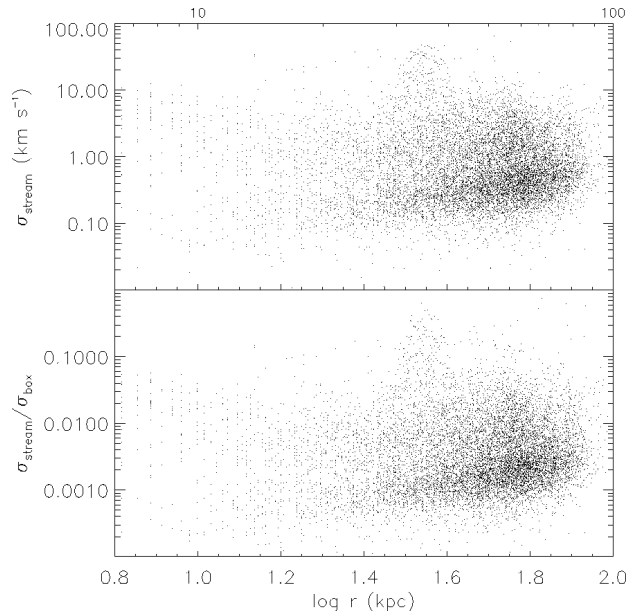


Figure 21. Mass-weighted velocity dispersions of streams inside cubic volumes located in the inner $([-60,+60])^3 \text{ kpc}^3$ of the galaxy halo. Boxes are 2 kpc on a side. In the bottom panel the velocities have been normalised to the 1-d total velocity dispersion inside the boxes at each r .

$$\sigma_{\text{stream}} = \sqrt{\frac{1}{N_T} \sum_{k=1,L} \frac{\sum_{ij} |\mathbf{v}_i - \mathbf{v}_j|^2}{N_k - 1}} \quad (14)$$

where the ij sum runs over all particle pairs in the k -th stream in a given box, N_k is the number of particles in this stream in this box, and as before, N_T is the total number of particles in the box. This mass-weighted velocity dispersion is expected to be relatively small in view of our results of the phase-space evolution of halo debris. We plot this quantity in Figure 21 as a function of distance from the galaxy centre for each one of the boxes considered. For our boxes of 2 kpc on a side we find a typical velocity dispersion of 1 km s^{-1} at the position of the “Sun”. The values observed are probably upper limits to the typical velocity dispersion in a stream, since they could only be measured for the densest streams (with two or more particles), and so are biased towards high velocity dispersions.

6 DISCUSSION

We have studied the phase-space evolution of debris from the progenitors that merge to build up a dark-matter halo in a Λ CDM cosmology. Our analysis has shown that the debris streams originating in progenitors of different sizes and orbital characteristics all behave in a similar way: with velocity dispersions and local space density decreasing in time. The evolution of the debris streams that we were able to follow until the present time is consistent with phase mixing. Even for halos that we could not follow for a very long time – because of their smaller initial number of particles or their shorter orbital timescales – we find the debris to show similar behaviour. On the scales of the fine-grained distribution function, mixing is apparently not strongly chaotic. On the

contrary, the phase-space evolution appears to be quite organised and simple, very similar to the mixing of streams orbiting in an idealised static potential.

In principle, a dark-matter halo formed in a Λ CDM cosmology is not a smooth entity. Not only do dark-matter halos contain a large number of dark satellites, they also have large amounts of substructure in the form of streams. We predict, however, that dark matter in the Solar neighbourhood should be clumped in a few hundred thousand streams, producing a velocity ellipsoid which is close to a multivariate Gaussian (Helmi, White & Springel 2002). These streams have their origin in the different halos that merged to form the dark halo of the Galaxy. Most of these halos give rise to a large number of intersecting streams in the inner Galaxy.

Determining the characteristics of these hundred thousand streams is difficult even with the high-resolution simulation used here. We are mostly limited by the number of particles. Although the simulation as a whole has 66 million particles, inside a 4 kpc box centred on the “Sun”, we find only a couple of thousand particles. In such boxes we find on average two hundred streams with more than one particle, and typically each has only two particles! The internal stream velocity dispersion that we measure at the present-day is extremely small, of the order of only 1 km s^{-1} .

It is encouraging that we find reasonable agreement between the behaviour of debris streams in static potentials and that observed in this high resolution simulation. This implies that our earlier estimates of the number of stellar streams in the vicinity of the Sun (Helmi & White 1999) may indeed apply. Since the initial stellar phase-space distribution in the progenitor objects was probably of lower dimensionality than we here assume – stars tend to form in disks so that the distribution in at least two of the six phase-space coordinates collapses – star streams may be colder than the dark matter streams we have analysed, and so may be more easily distinguishable. It is also interesting to note that because the material that ends up populating the inner galaxy was already in place 10 Gyr ago, the oldest stars are predicted to be near the galactic centre (White & Springel 2000). Because this material comes from only a few objects, one might expect the stellar populations to be quite homogeneous, although this of course depends on whether the stars themselves formed in these few massive objects, or whether they were accreted into these objects in the first place.

A crude estimate of the stellar content of a stream in the Solar neighbourhood can be obtained as follows. Let us first estimate the “mass-to-light” ratio per particle $[M_{\text{DM}}/L_*]$ as the ratio of dark-matter mass to stellar halo light enclosed in a shell of thickness 2 kpc at the location of the Sun. We use the NFW profile of Eq.(3) for the dark-matter distribution. For the stellar distribution we assume a density profile $\rho_*(r) = \rho_{\odot} r_{\odot}^2 / (r^3 + r_c^3)$, where $\rho_{\odot} \sim 3 \times 10^4 M_{\odot} \text{ kpc}^{-3}$, and where r_c is the core radius, and is much smaller than r_{\odot} . We obtain for the Solar Neighbourhood $[M_{\text{DM}}/L_*] \sim 625$, for $\Upsilon_* = 2.5\Upsilon_{\odot}$. For one of our most massive streams (with 3 particles), this would imply an average $\sim 0.54 M_{\odot}$ in stars in a sphere of 100 pc radius centred on the Sun. Assuming a Salpeter initial mass function, and down to an absolute magnitude of $M_V = 7^m$ (Bergbusch & Vandenberg 1992), i.e. $V = 12^m$ at a distance of 100 pc, this corresponds to approximately 2 stars per stream. On the other hand, streams originate from very localised regions of phase-space in the

progenitor objects, so it seems more likely that only about one stream in 250 has any stars at all, that these streams have $\Upsilon_* = 2.5$ characteristic of the “stellar” regions of their progenitors, and that all the other streams are dark. In this case a massive, “luminous” stream might contain $135 M_{\odot}$ in stars in a sphere of 100 pc radius centred on the Sun, implying approximately 450 stars down to $M_V = 7^m$ for a Salpeter IMF.

More reliable estimates of the stellar content and number of streams, as well as considerably more insight into the properties of the Galactic stellar halo would be obtained by combining semi-analytic techniques (e.g Kauffmann et al. 1993) with high-resolution simulations (see, for example, Springel et al. 2001). This would enable one to predict trends in the chemical composition, age, spatial distribution and kinematics of halo stars as a function of position throughout the Galaxy.

ACKNOWLEDGMENTS

We wish to thank the referee for the positive remarks which helped us improve this manuscript.

REFERENCES

- Benson A. J., Frenk C. S., Baugh C. M., Cole S., Lacey C. G., 2001, MNRAS, 327, 1041
 Benson A. J., Frenk C. S., Lacey C. G., Baugh C. M., Cole S., 2002, MNRAS, 333, 177
 Bergbusch P.A., Vandenberg D.A., 1992, ApJS, 81, 163
 Binney J., Tremaine S., 1987, Galactic Dynamics. Princeton University Press, Princeton, NJ
 Bode P., Ostriker J. P., Turok N., 2001, ApJ, 556, 93
 Bullock J.S., Kravtsov A., Weinberg D.H., 2001, ApJ, 548, 33
 Dejonghe H., de Zeeuw P.T., 1988, ApJ, 333, 90
 de Zeeuw P.T., 1985, MNRAS, 216, 273
 Diaferio A., Kauffmann G., Balogh M. L., White S. D. M., Schade D., Ellingson E., 2001, MNRAS, 323, 999.
 Dohm-Palmer R.C., Helmi A., Morrison H., Mateo M., Olszewski E.W., Harding P., Freeman K.C., Norris J., Shectman S. A., 2001, ApJ, 555, L37
 Ghigna S., Moore B., Governato F., Lake G., Quinn T., Stadel J., 2000, ApJ, 544, 616
 Goldstein H., 1953, Classical Mechanics, Addison-Wesley, Cambridge, Mass.
 Helmi A., White S.D.M, 1999, MNRAS, 307, 495
 Helmi A., White S.D.M, de Zeeuw P.T., Zhao H.S., 1999, Nature, 402, 53
 Helmi A., White S.D.M, 2001, MNRAS, 323, 529
 Helmi A., White S.D.M, Springel V., 2002, Phys.Rev.D 66, 063502 327, 329
 Ibata R., Irwin M., Lewis G. F., Stolte A., 2001, ApJ, 547, L133
 Ibata R., Lewis G., Irwin M., Quinn T., 2002, MNRAS, 332, 915
 Ivezić Z., et al. (SDSS), 2000, AJ, 120, 963
 Jing Y.P., Suto Y., 2000, ApJ, 529, L69
 Johnston K.V., Hernquist L., Bolte M., 1996, ApJ, 465, 278
 Johnston K.V., 1998, ApJ, 495, 297
 Johnston K.V., Spergel D., Haydn C., 2002, ApJ, 570, 656
 Kamionkowski M., Liddle A., 2000, Phys. Rev. Lett, 84, 4525
 Kauffmann G., White S.D.M., Guiderdoni B., 1993, MNRAS, 264, 201
 Kauffmann, G., Colberg, J. M., Diaferio, A., White, S. D. M. 1999, MNRAS, 303, 188

- Kleyna, J., Wilkinson, M. I., Evans, N. W., Gilmore, G., Frayn, C. 2002, MNRAS, 330, 792
- Klypin A., Kravtsov A., Valenzuela O., Prada F., 1999, ApJ, 522, 82
- Klypin A., Zhao H., Somerville R., 2002, astro-ph/0110390
- Lacey C., Cole S., 1993, MNRAS, 262, 627
- Lokas E. L., 2001, MNRAS, 327, L21
- Lynden-Bell D., 1962, MNRAS, 124, 2, 9
- Martínez-Delgado D., Aparicio A., Gómez-Flechoso M.A., Carrera R., 2001, ApJ, 549, L199
- Mateo M., 1997, ASP Conf. Ser. 116: The Nature of Elliptical Galaxies; 2nd Stromlo Symposium, 259.
- Mayer L., Moore B., Quinn T., Governato F., Stadel J., 2002, astro-ph/0110386
- Moore B., Ghigna S., Governato F., Lake G., Quinn T., Stadel J., Tozzi P., 1999, ApJ, 524, L19
- Navarro J.F., Frenk C.S., White S.D.M., 1996, ApJ, 462, 563
- Somerville R. S., Primack J. R., Faber S. M., 2001, MNRAS, 320, 504
- Spergel D. N., Steinhardt P. J., 2000, Physical Review Letters, 84, 3760
- Springel V., White S.D.M., Tormen G., Kauffmann G., 2001, MNRAS, 328, 726
- Springel V., Yoshida N., White S.D.M., 2001, New Astronomy, 6, 79
- Stoehr F., White S.D.M., Tormen G., Springel V., 2002, MNRAS (in press), astro-ph/0203342
- Tormen G., Bouchet F.R., White S.D.M., 1997, MNRAS, 286, 865
- van den Bosch F.C., 2002, MNRAS, 331, 98
- Vivas A.K., et al. (QUEST), 2001, ApJ, 554, L33
- Wechsler R. H., Bullock J. S., Primack J. R., Kravtsov A. V., Dekel, A., 2002, ApJ, 568, 52
- White S.D.M., Rees M.J., 1978, MNRAS, 183, 341
- White S.D.M., Springel V., 2000, in The First Stars, Proceedings of the MPA/ESO Workshop held at Garching, Germany, 4-6 August 1999; eds. Weiss, Abel & Hill (Springer), 327
- Yanny B. et al. (SDSS), 2000, ApJ, 540, 825
- Zhao D., Mo H., Jing Y.P., Boerner G., 2002, astro-ph/0204108